# Identifying the Circular Polarization Handedness of an Antenna in a Reverberation Chamber

Qian Xu, Lei Xing, Yongjiu Zhao, Tianyuan Jia and Yi Huang

***Abstract*—When an antenna is circularly (or elliptically) polarized, the axial ratio can be measured in a reverberation chamber (RC) by using the self-correlation of the radiation pattern of the antenna under test (AUT). However, the self-correlation method cannot identify the handedness (left- or right-handed polarization) of an antenna. In this paper, we propose a reference antenna method in an RC to solve this problem. Two reference antennas are used, which are right-handed and left-handed circularly polarized, respectively. By measuring the radiation pattern correlation between the AUT and the reference antennas, the handedness of the AUT can be identified. Interestingly, the results are based on statistics and the significance of the measurement results is self-explained. Measurements are performed to validate the proposed method.**

***Index Terms*—antenna measurement, reverberation chamber, circular polarization.**

## I. Introduction

A reverberation chamber (RC) is a highly resonant and electrically large cavity. In an RC, a rich isotropic multipath (RIMP) environment is naturally created, and the electromagnetic (EM) fields can be redistributed by changing the boundary conditions (mechanical stir), source position (source stir) or the signal frequency (frequency stir) [1-6]. The applications of RCs have been extended widely in recent years, from classical electromagnetic compatibility (EMC) area [1] to antenna measurement and over-the-air (OTA) system test [2-6]. In antenna or antenna array measurements, typical applications include and may not limited to radiation efficiency [7-11], free-space *S*-parameters [12], mutual coupling [13], diversity gain [13-15], radiation pattern correlation [16-18], radiation pattern reconstruction [18-21] and axial ratio (AR) measurement [18].

Unlike in free space (or in an anechoic chamber), in an RIMP environment, the directional property of an antenna is easily submerged by the multipath interference since the waves are diffused randomly. To obtain the directional properties, we have to apply specific strategies to retain the coherent part and remove the incoherent component. Typical applications include radiation pattern reconstruction using *K*-factors [21] and free-space *S*-parameter measurement [12]. However, the RIMP environment has many advantages, the diffused wave makes it very suitable for measuring global properties, such as shielding effectiveness [1, 22-24], average absorption cross section [25-27], total scattering cross section [28-30], radiation efficiency [7-11], total radiated power [31, 32], total isotropic sensitivity [33-35] and correlation coefficient [16-18]. It is interesting to note that, these global properties can be measured directly without knowing the angle dependencies, which makes the measurement setup in an RIMP environment very robust, i.e. the antenna or the device under test does not have to be aligned and aimed carefully and accurately in a line-of-sight (LoS) way.

Manuscript received November 25, 2019. This work was supported in part by the National Natural Science Foundation of China under Grants 61701224 and 61601219.

Q. Xu, L. Xing, Y. Zhao are with College of Electronic and Information Engineering, Nanjing University of Aeronautics and Astronautics, Nanjing 211106, China (e-mail: emxu@foxmail.com).

T. Jia and Y. Huang is with the Department of Electrical Engineering and Electronics, The University of Liverpool, Liverpool L69 3GJ, UK. (e-mail: yi.huang@liverpool.ac.uk).

Specifically, we have shown the measurement of an antenna radiation pattern and the axial ratio (AR) measurement in an RC [18], the measurement setup does not require the AUT to be aligned to a receiving (Rx) or transmitting (Tx) antenna. The radiation pattern (or AR) can be reconstructed from the self-correlation of an AUT. However, for a circularly polarized (CP) AUT, the measurement process cannot distinguish if the CP is left-handed (RH) or right-handed (LH). If the LH/RH switching is used in a communication system, only the AR measurement cannot distinguish the handedness of the source. Although the AR can be measured accurately, the handedness of the CP has not been identified yet. In this work, we propose a reference antenna method to solve this problem. By measuring the correlation of the AUT and the reference antennas, the handedness of the AUT can be identified.

In Section II, the principle of the method is presented. Section III details the measurement results and Section IV summarizes the discussion and conclusions.

## II. Theory

It has been found that the self-correlation of a radiation pattern of an antenna can be measured in an RC without knowing the details of the radiation pattern [18]. Suppose $\mathbf{E}_1(\theta,\varphi)$ is the farfield radiation pattern of Ant 1 in Fig. 1, $\mathbf{E}_{\gamma 1}(\theta,\varphi)$ is a rotated version of $\mathbf{E}_1(\theta,\varphi)$ around $z$-axis with a rotation angle of $\gamma$, $S_{21}$ is a set of *S*-parameters measured between Ant 1 and Ant 2 for different frequencies (frequency stir) or different stirrer positions (mechanical stir), and $S_{\gamma 21}$ is a set of *S*-parameters measured in the same scenario when Ant 1 is rotated by an angle $\gamma$. From the previous study [18], we know that the correlation of a radiation pattern can be measured using the correlation of *S*-parameters in a RIMP environment [16-18]:

$$
\begin{aligned}
&corr\left(S_{21}, S_{\gamma 21}\right) \\
&= \frac{\left|\sum_{k=1}^{N}[S_{21}(k)-\langle S_{21}\rangle][S_{\gamma 21}(k)-\langle S_{\gamma 21}\rangle]^*\right|}{\sqrt{\sum_{k=1}^{N}|S_{21}(k)-\langle S_{21}\rangle|^2 \sum_{k=1}^{N}\left|S_{\gamma 21}(k)-\langle S_{\gamma 21}\rangle\right|^2}} \\
&= \frac{\left|\iint \mathbf{E}_1(\theta,\varphi)\cdot\mathbf{E}_{\gamma 1}^*(\theta,\varphi)d\Omega\right|}{\sqrt{\iint|\mathbf{E}_1(\theta,\varphi)|^2 d\Omega \iint\left|\mathbf{E}_{\gamma 1}^*(\theta,\varphi)\right|^2 d\Omega}} = corr\left(\mathbf{E}_1, \mathbf{E}_{\gamma 1}\right)
\end{aligned} \tag{1}
$$

where $N$ represents the measured sample number, $\langle\cdot\rangle$ means the average operation over $N$ samples, and $\iint \blacksquare\, d\Omega = \int_0^{2\pi}\int_0^{\pi} \blacksquare\, sin\theta\, d\theta\, d\varphi$ represents the integral over a unit spherical surface, $\theta$ is the polar angle and $\varphi$ is the azimuth angle.

It has been shown that the AR can be measured from the minimum value of the correlation for different angles [18]. However, if we check the AR measurement process carefully, we can find that this method leads the same angular correlation for both clockwise and anti-clockwise rotation of the AUT. Because the angle $\gamma$ is a relative value, the positive and negative rotation leads the same angular correlation. We cannot extract more information from a single axis of rotation of AUT, unless the rotation is combined with other axis (more than one axis of rotation).

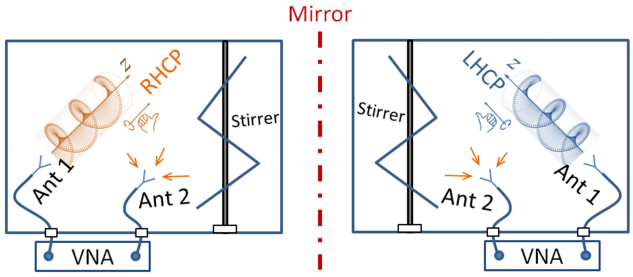


(a) (b)

Fig. 1. A schematic plot of thought experiment, (b) is a mirrored scenario of (a). An RHCP antenna is transformed into an LHCP antenna in mirror.

If we take a symmetric transform of the measurement system in Fig. 1(a), Fig. 1(b) is obtained. Since the law of physics inside the mirror is the same as that outside the mirror (we are still in the region of classical physics), we have the same measured *S*-parameters. Thus we have the same angular correlations for the RHCP and LHCP antenna, although in the mirror the RHCP antenna has been transformed into an LHCP one.

As can be seen, use only one axis of rotation without other antennas is impossible to distinguish the state of CP. Use more than one axis is possible [18], but we have to make sure that all the rotations in sequence share the same reference point of the 3D pattern. Otherwise, a 3D pattern transformation is required which would further increase the complexity of the measurement. To solve this problem, we introduce two reference antennas of which the helicities are known as shown in Fig. 2. $\mathbf{E}_{\text{Rref}}(\theta,\varphi)$ and $\mathbf{E}_{\text{Lref}}(\theta,\varphi)$ are the radiation patterns of the RHCP and the LHCP reference antennas respectively, and $\mathbf{E}_{\text{AUT}}(\theta,\varphi)$ is the radiation pattern of the AUT. Similar to the AR derivation in [18], we can ignore the contribution except the main lobe in +$z$-axis. Suppose the AUT is LHCP, in +$z$-axis we have

$$\mathbf{E}_{\text{AUT}} = E_x\hat{a}_x + jE_y\hat{a}_y \tag{2}$$

where $\hat{a}_x$ and $\hat{a}_y$ are unit vectors in $x$- and $y$- directions respectively. The plane waves related to the emission of the LHCP and RHCP reference antennas in +$z$-axis are

$$\mathbf{E}_{\text{Lref}} = E_r\hat{a}_x + jE_r\hat{a}_y \tag{3}$$
$$\mathbf{E}_{\text{Rref}} = E_r\hat{a}_x - jE_r\hat{a}_y \tag{4}$$

The correlation between $\mathbf{E}_{\text{AUT}}(\theta,\varphi)$ and $\mathbf{E}_{\text{Lref}}(\theta,\varphi)$ can be approximated as (when the AUT is rotated with an angle $\gamma$)

$$corr(\mathbf{E}_{\text{AUT}},\ \mathbf{E}_{\text{Lref}}) \approx \frac{\left|\begin{bmatrix}cos\gamma & -sin\gamma\\ sin\gamma & cos\gamma\end{bmatrix}\begin{bmatrix}E_x\\ jE_y\end{bmatrix}\cdot\begin{bmatrix}E_r\\ jE_r\end{bmatrix}^*\right|}{\sqrt{E_x^2+E_y^2}\sqrt{2E_r^2}} = \frac{|E_x+E_y|}{\sqrt{E_x^2+E_y^2}\sqrt{2}} \tag{5}$$

and the correlation between $\mathbf{E}_{\text{AUT}}(\theta,\varphi)$ and $\mathbf{E}_{\text{Rref}}(\theta,\varphi)$ can be approximated as

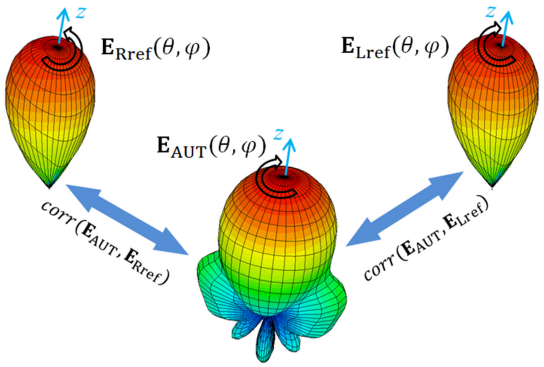


Fig. 2. The radiation pattern correlations between the AUT and the reference antennas with RHCP and LHCP, respectively.

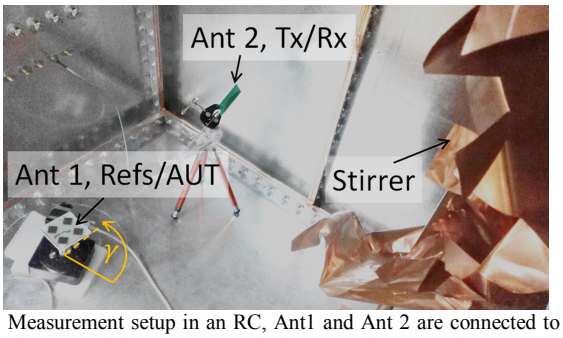


Fig. 3. Measurement setup in an RC, Ant1 and Ant 2 are connected to the port 1 and port 2 of the VNA respectively; Ant 1 is mounted on a turntable. The dimensions of the RC are 0.8 m × 1.2 m × 1.2 m.

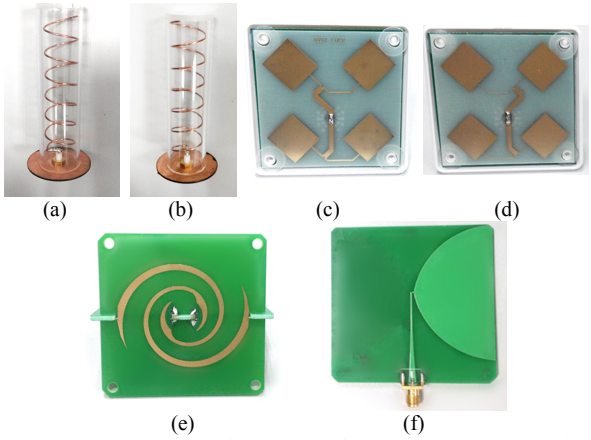

(a) (b) (c) (d) (e) (f)

Fig. 4. Antennas connect to the port 1 of the VNA, (a) an LHCP reference antenna, (b) an RHCP reference antenna, (c) AUT #1, an LHCP AUT (patch antenna array), (d) AUT #2, an RHCP AUT (patch antenna array), (e) AUT #3, an RHCP AUT (spiral antenna), (f) AUT #4, a linearly polarized AUT.

$$corr(\mathbf{E}_{\text{AUT}},\ \mathbf{E}_{\text{Rref}}) \approx \frac{\left|\begin{bmatrix}cos\gamma & -sin\gamma\\ sin\gamma & cos\gamma\end{bmatrix}\begin{bmatrix}E_x\\ jE_y\end{bmatrix}\cdot\begin{bmatrix}E_r\\ -jE_r\end{bmatrix}^*\right|}{\sqrt{E_x^2+E_y^2}\sqrt{2E_r^2}} = \frac{|E_x-E_y|}{\sqrt{E_x^2+E_y^2}\sqrt{2}} \tag{6}$$

The derivations are similar for an RHCP AUT, we only need to replace $E_y$ with $-E_y$ in (5) and (6). Since (5) and (6) are different for RHCP or LHCP AUT, the handedness of the AUT can be identified. E.g. if $corr(\mathbf{E}_{\text{AUT}},\ \mathbf{E}_{\text{Lref}}) > corr(\mathbf{E}_{\text{AUT}},\ \mathbf{E}_{\text{Rref}})$, the AUT is LH polarized; if $corr(\mathbf{E}_{\text{AUT}},\ \mathbf{E}_{\text{Lref}}) < corr(\mathbf{E}_{\text{AUT}},\ \mathbf{E}_{\text{Rref}})$, the AUT is RH polarized. However, this criterion cannot give information of the

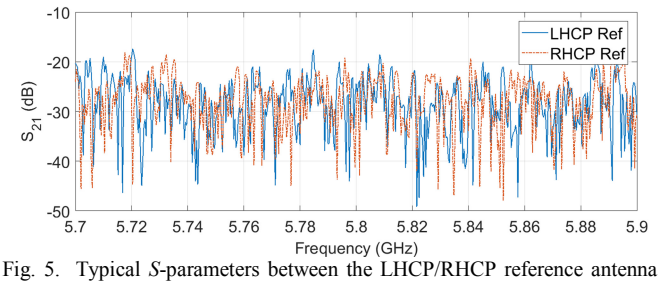


Fig. 5. Typical *S*-parameters between the LHCP/RHCP reference antenna (port 1) and the Tx antenna (port 2) at one $\gamma$ angle.

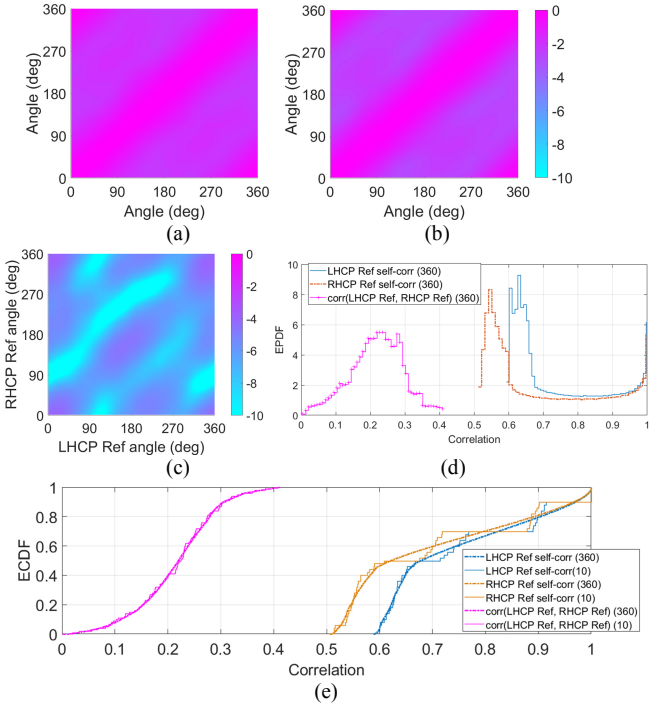


Fig. 6. (a) Measured self-correlation of the LHCP reference antenna: $corr\left(\mathbf{E}_{\gamma_1\mathrm{Lref}}, \mathbf{E}_{\gamma_2\mathrm{Lref}}\right)$, $\mathbf{E}_{\gamma_1\mathrm{Lref}}$ means the radiation pattern of the LHCP reference antenna is rotated with an angle of $\gamma_1$ in $z$-axis; (b) measured self-correlation of the RHCP reference antenna: $corr\left(\mathbf{E}_{\gamma_1\mathrm{Rref}}, \mathbf{E}_{\gamma_2\mathrm{Rref}}\right)$; (c) measured correlation between the LHCP and RHCP reference antenna: $corr\left(\mathbf{E}_{\gamma_1\mathrm{Lref}}, \mathbf{E}_{\gamma_2\mathrm{Rref}}\right)$, $10\log_{10}$ is used to convert linear unit to dB unit. (d) EPDF plots of the measured correlations with 360 $\gamma$ angles; (e) ECDF plots of the measured correlations with 360 and 10 $\gamma$ angles.

significance of the measurement results, and we present the significance together with measurement data in the next section.

## III. Measurements

The measurement setup is illustrated in Fig. 3. We perform the measurements in three steps:

1) Record the *S*-parameters or channel state information (CSI) for the LHCP reference antenna;
2) Replace the LHCP reference antenna in step 1) with the RHCP reference antenna and repeat the same measurement procedure;
3) Replace the RHCP reference antenna in step 2) with the AUT and repeat the same measurement procedure.

Note that step 1) and 2) only need to be measured once. In Fig. 3, port 1 is connected to the reference antennas (LHCP or RHCP) or AUTs, port 2 is connected to a Tx (or Rx) antenna respectively. The reference antennas and the AUTs (#1 ~ #4) are shown in Fig. 4. We use two helical antennas as the reference antennas. The working frequency of the antennas is 5.8 GHz (the antennas are used for first-

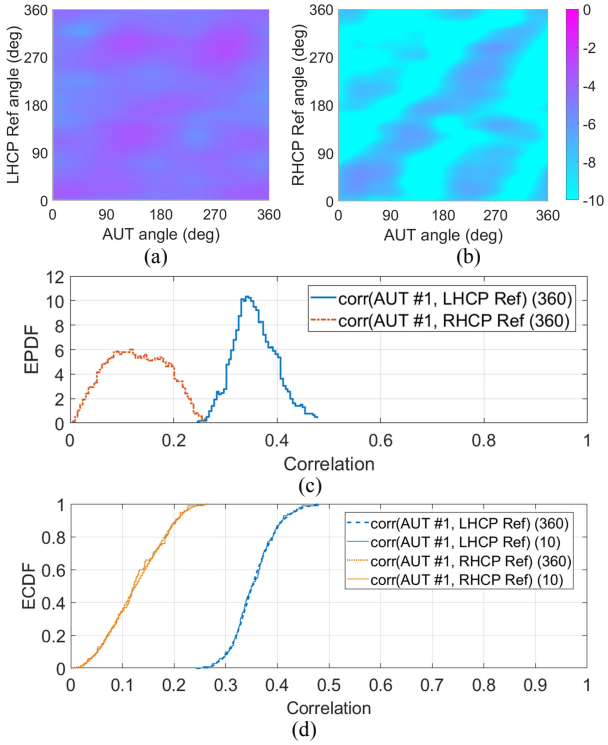


Fig. 7. (a) Measured correlation between AUT #1 and the LHCP reference antenna; (b) measured correlation between AUT #1 and the RHCP reference antenna; (c) EPDF plots of the measured correlations; (d) ECDF plots of the measured correlations with 360 and 10 $\gamma$ angles.

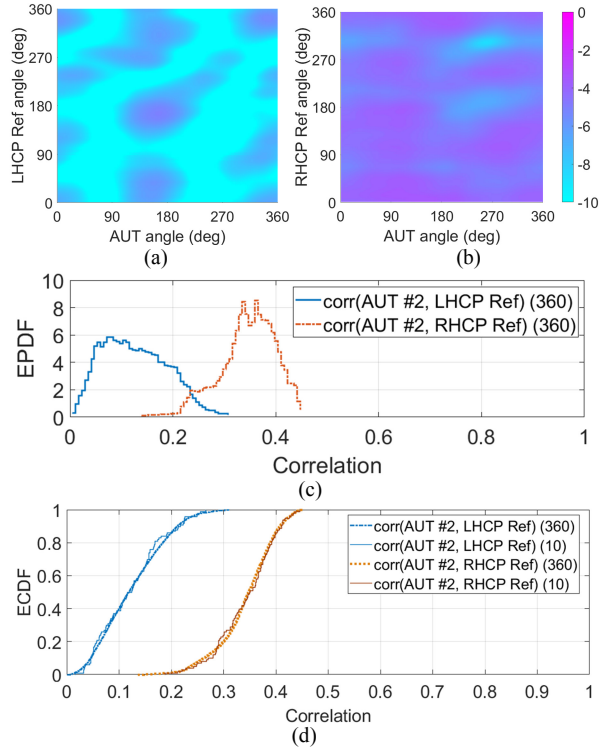


Fig. 8. (a) Measured correlation between AUT #2 and the LHCP reference antenna; (b) measured correlation between AUT #2 and the RHCP reference antenna; (c) EPDF plots of the measured correlations; (d) ECDF plots of the measured correlations with 360 and 10 $\gamma$ angles.

person view remote-control flying). *S*-parameters of 501 frequency points are measured in the frequency range of 5.7 GHz – 5.9 GHz. Typical *S*-parameters at one rotation angle of the reference antennas

and Tx antenna are shown in Fig. 5, the measured $S_{21}$ is well above the noise level of the VNA which is about -100 dB. We rotate the antenna connected to port 1 of the VNA with 1°/step, the measured $S_{21}$ are used to calculate the correlations between the reference antennas and the AUT.

To verify the measurement setup in Fig. 1, we measure the self-correlation [18] of the LHCP and RHCP reference antennas. All the measured *S*-parameters in the frequency range of 5.7 GHz – 5.9 GHz are used to calculate the self-correlations between any pair of two rotation angles; the calculation process is very similar to the stirrer correlation for mechanical stirrers in [36]. The measured correlations in dB are presented in Fig. 6. As can be seen in Fig. 6(a) and (b), we have very similar plots for the self-correlations for the LHCP and RHCP reference antennas, as expected, this means that we cannot identify the handedness from the self-correlations.

In the meanwhile, since the two reference antennas have an opposite handedness, the correlations between these two antennas show small values for different rotation angles (in Fig. 6(c)). Correlation values in Fig. 6(a)-(e) are used to plot the empirical probability density functions (EPDFs) and the empirical cumulative distribution functions (ECDFs), and the results are illustrated in Fig. 6(e). The results using only 10 $\gamma$ angles are also presented, in which they agree well with that using 360 $\gamma$ angles. Suppose we have an AUT which is exactly the same as the RHCP (or LHCP) reference antenna, we can obtain high correlations with RHCP (or LHCP) reference antenna and small correlations with LHCP (or RHCP) reference antenna. Thus the handedness of the AUT can be identified from Fig. 6(d) and (e).

To verify the proposed method, we measure the correlations between the AUTs (#1 ~ #4) and the reference antennas. AUT #1 and #2 are patch antennas and the bandwidth is narrower than AUT #3 which is a spiral antenna. The results are presented in Fig. 7-Fig. 10. As can be seen, the handedness of the AUTs can be well identified in Fig. 7 - Fig. 9, and the EPDFs of the correlations between the AUTs and the reference antennas show significant difference. Note that AUT #3 is a wideband CP antenna; the correlations in Fig. 9(c) are separated wider than that in Fig. 7(c) and Fig. 8(c). In Fig. 10, since AUT #4 is a linearly polarized antenna (a wideband dipole), the correlations for the reference antennas are both small and the EPDFs have significant overlapped region. Thus the handedness of AUT #4 is neither LHCP nor RHCP.

Note that the correlation EPDFs and ECDFs in Fig. 10(c) and (d) are not exactly the same, this should be due to the imperfect symmetry between the LHCP and the RHCP reference antennas. This can also be observed in the self-correlations in Fig. 6(e). We have also measured the ARs of the antennas in Fig. 4 using the method in [18]. The results are presented in Fig. 11, in which we can also find that the ARs of the LHCP and the RHCP reference antennas are not exactly the same. Although the reference antennas are not perfectly symmetric, they do not affect the use of them.

## IV. Discussion

We have shown that the handedness of the AUT can be identified using the reference antenna method, and the significance of the measurement results is self-explained with EPDFs. However, we have to note that there is a precondition in the measurement: the reference points of the radiation pattern of the AUT and the reference antennas are the same. We know that in an RC, when an antenna is moved in a certain distance, independent *S*-parameters can be obtained [2]. If the reference point shifts, will the results be affected?

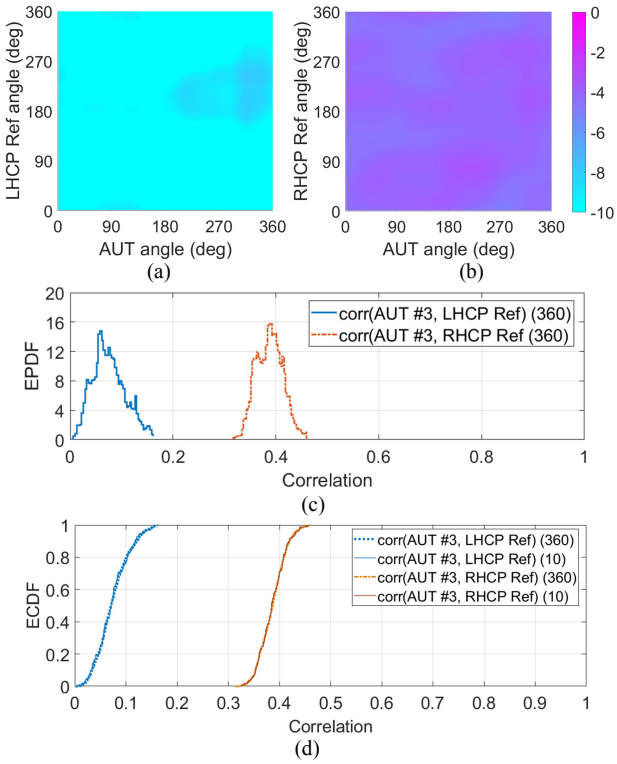


Fig. 9. (a) Measured correlation between AUT #3 and the LHCP reference antenna; (b) measured correlation between AUT #3 and the RHCP reference antenna; (c) EPDF plots of the measured correlations; (d) ECDF plots of the measured correlations with 360 and 10 $\gamma$ angles.

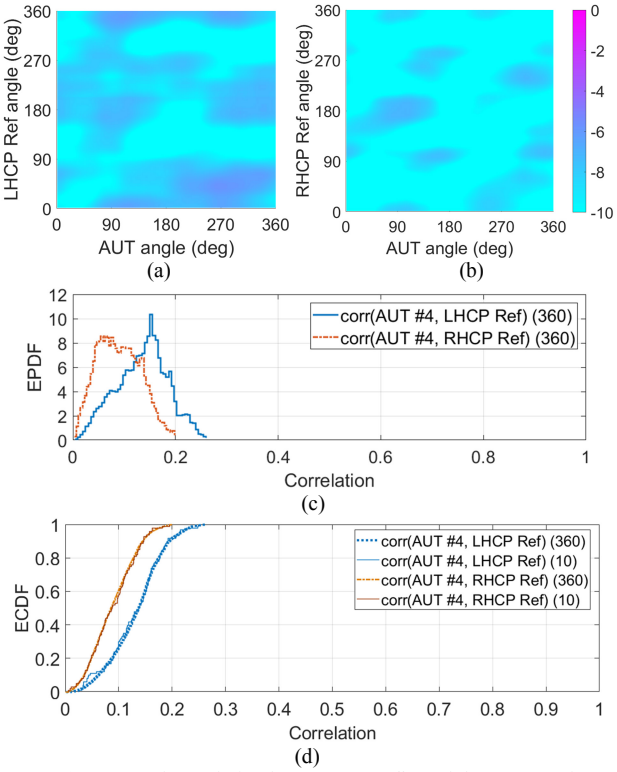


Fig. 10. (a) Measured correlation between AUT #4 and the LHCP reference antenna; (b) measured correlation between AUT #4 and the RHCP reference antenna; (c) EPDF plots of the measured correlations; (d) ECDF plots of the measured correlations with 360 and 10 $\gamma$ angles.

We note that AUT #1 - #3 may not have the same reference points with the reference antennas, but the results are still significant. To

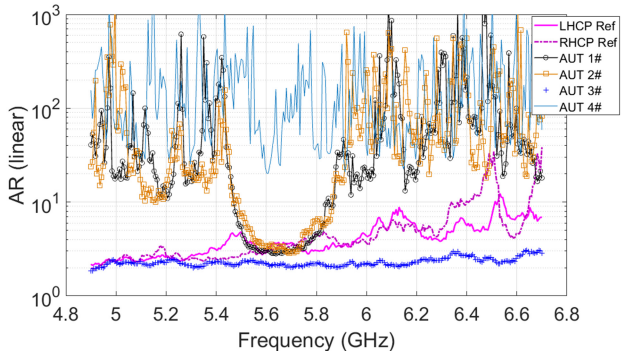


Fig. 11. Measured ARs of antennas in Fig. 4 in an RC.

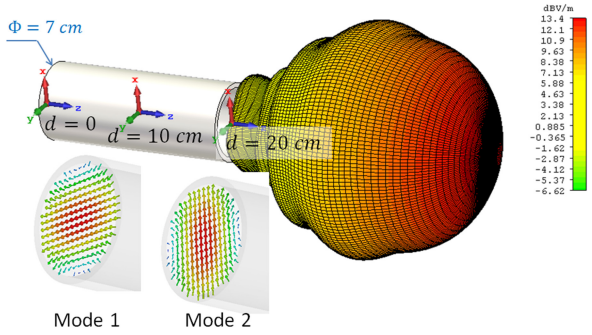


Fig. 12. A horn antenna excited with two orthogonal modes simultaneously, the two orthogonal modes are shown with a phase difference of 90° at 3 GHz.

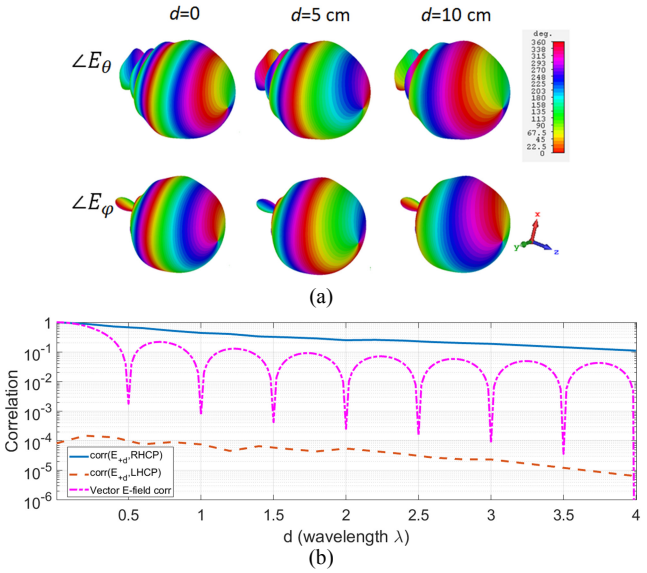


Fig. 13. (a) Phase distribution of the polar component and the azimuth component of the radiated E-field for different shift distance $d$, (b) simulated correlations between the shifted radiation patterns and the RHCP/LHCP reference patterns, the vector E-field correlation $(\sin(kd)/kd)$ is also given.

quantify this effect, a horn antenna is simulated with different reference point for the radiation pattern. The model is illustrated in Fig. 12, in which the CP is realized by using two orthogonal modes excited simultaneously with a 90° phase difference. Both RHCP and LHCP can be realized by using +90° or -90° phase difference. We shift the original point in +$z$-axis with different distances ($d$ in Fig. 12) and simulate the radiation patterns with different $d$, the results are illustrated in Fig. 13. As can be seen in Fig. 13(a), the phase of the polar component and the azimuth component is redistributed for different $d$. In Fig. 13(b), we use the original RHCP and LHCP radiation patterns as the references and calculate the correlations between the transformed radiation patterns and reference ones ($corr(\mathrm{E}_{+d}, \mathrm{RHCP})$ and $corr(\mathrm{E}_{+d}, \mathrm{LHCP})$ in Fig. 13(b)). As can be seen, when the shift distance is not large ($< 3\lambda$), the correlations between the RHCP and LHCP are separated clearly which means the handedness can be identified significantly. The vector E-field correlation [2] is also presented; it is interesting to note that the correlation of a directional CP antenna is larger than the vector E-field correlation.

Another thing to note is that in the measurement process for $corr(\mathrm{AUT}, \mathrm{LHCP\ Ref})$ and $corr(\mathrm{AUT}, \mathrm{RHCP\ Ref})$, the position of Ant 2, the position of the turntable and the stirring sequence must be the same. Otherwise when the multipath environment is changed, we have two independent measurement scenarios, and the measured results will be decorrelated.

## V. Conclusions

Although the AR can be measured in an RC, the handedness cannot be identified using a single antenna with a single axis of rotation. We have proven the infeasibility of the methodology using only one axis of rotation (in a virtual experiment), and demonstrated it in measurements. This leads the proposed reference antenna method.

The proposed method is based on the correlation of the radiation pattern, and the radiation pattern does not have to be measured angle by angle in free space. The measurement time is very similar to the antenna efficiency or TRP measurement. After the reference antennas have been measured, for the AUT measurement in this work, it takes about 20 minutes for 360 $\gamma$ angles and less than 1 minute for 10 $\gamma$ angles respectively. Different types of AUTs have been used to verify the proposed method. The measurement results are presented in the form of EPDFs and ECDFs which are self-explained: the more difference in EPDF and ECDF plots, the more significant the result is. The measurement setup in an RC is very robust and does not require careful alignment between the AUT and the Tx/Rx antenna. The effect of the reference point shift has also been investigated, which shows that when the shift of the reference point is small ($< 3\lambda$) the proposed method is still significant.

## References

[1] IEC 61000-4-21, *Electromagnetic compatibility (EMC) – Part 4-21: Testing and measurement techniques – Reverberation chamber test methods,* IEC Standard, Ed 2.0, 2011-01.

[2] D. A. Hill, *Electromagnetic Fields in Cavities: Deterministic and Statistical Theories*, Wiley-IEEE Press, USA, 2009.

[3] P. Besnier and B. Demoulin, *Electromagnetic Reverberation Chambers*, Wiley-ISTE, UK, 2011.

[4] S. J. Boyes, Y. Huang, *Reverberation Chambers, Theory and Applications to EMC and Antenna Measurements*, Wiley, UK, 2016

[5] Q. Xu and Y. Huang, *Anechoic and Reverberation Chambers: Theory, Design and Measurements*, Wiley-IEEE, UK, 2019.

[6] CTIA, *Test Plane for Wireless Large-Form-Factor Device Over-the-Air Performance*, Ed 1.1, 2017-07.

[7] C. L. Holloway, H. A. Shah, R. J. Pirkl, W. F. Young, D. A. Hill and J. Ladbury, "Reverberation chamber techniques for determining the radiation and total efficiency of antennas," *IEEE Transactions on Antennas and Propagation*, vol. 60, no. 4, pp. 1758-1770, Apr. 2012.

[8] X. Chen, "On statistics of the measured antenna efficiency in a reverberation chamber," *IEEE Transactions on Antennas and Propagation*, vol. 61, no. 11, pp. 5417-5424, Nov. 2013.

[9] Q. Xu, Y. Huang, X. Zhu, L. Xing, Z. Tian and C. Song, "A modified two-antenna method to measure the radiation efficiency of antennas in a reverberation chamber," *Antennas and Wireless Propagation Letters IEEE*, vol. 15, pp. 336-339, 2016.

[10] S. J. Boyes, Y. Zhang, A. K. Brown and Y. Huang, "A method to de-embed external power dividers in efficiency measurements of all-excited

antenna arrays in reverberation chamber," *IEEE Antennas and Wireless Propagation Letters*, vol. 11, pp. 1418-1421, 2012.
[11] Z. Tian, Y. Huang and Q. Xu, "An improved method for efficiency measurement of all-excited antenna array in reverberation chamber using power divider," *IEEE Transactions on Antennas and Propagation*, vol. 65, no. 6, pp. 3005-3013, Jun. 2017.
[12] P. -S. Kildal, C. Carlsson and J. Yang, "Measurement of free-space impedances of small antennas in reverberation chambers," *Microwave and Optical Technology Letters*, vol. 32, no. 2, pp. 112-115, Jan. 2002.
[13] P. -S. Kildal and K. Rosengren, "Correlation and capacity of MIMO systems and mutual coupling, radiation efficiency, and diversity gain of their antennas: simulations and measurements in a reverberation chamber," *IEEE Communications Magazine*, vol. 42, no. 12, pp. 104-112, Dec. 2004.
[14] K. Rosengren and P. -S. Kildal, "Radiation efficiency, correlation, diversity gain and capacity of a six-monopole antenna array for a MIMO system: theory, simulation and measurement in reverberation chamber," *IEE Proceedings - Microwaves, Antennas and Propagation*, vol. 152, no. 1, pp. 7-16, Feb. 2005.
[15] J. Yang, S. Pivnenko, T. Laitinen, J. Carlsson and X. Chen, "Measurements of diversity gain and radiation efficiency of the eleven antenna by using different measurement techniques," *4th European Conference on Antennas and Propagation (EuCAP)*, pp.1-5, 12-16 Apr. 2010.
[16] X. Chen, P. -S. Kildal and J. Carlsson, "Comparisons of different methods to determine correlation applied to multi-port UWB eleven antenna," *5th European Conference on Antennas and Propagation (EuCAP)*, pp.1776-1780, 11-15 Apr. 2011.
[17] P. Hallbjorner, "Accuracy in reverberation chamber antenna correlation measurements," *International Workshop on Antenna Technology: Small and Smart Antennas Metamaterials and Applications (IWAT)*, pp.170-173, 21-23 Mar. 2007.
[18] Q. Xu, Y. Huang, L. Xing, C. Song, Z. Tian, S. S. Alja'afreh and M. Stanley, "3-D antenna radiation pattern reconstruction in a reverberation chamber using spherical wave decomposition," *IEEE Transactions on Antennas and Propagation*, vol. 65, no. 4, pp. 1728-1739, Apr. 2017.
[19] A. Cozza and A. el-Aileh, "Accurate radiation-pattern measurements in a time-reversal electromagnetic chamber," *IEEE Antennas and Propagation Magazine*, vol. 52, no. 2, pp. 186-193, Apr. 2010.
[20] V. Fiumara, A. Fusco, V. Matta and I. M. Pinto, "Free-space antenna field/pattern retrieval in reverberation environments," *IEEE Antennas and Wireless Propagation Letters*, vol. 4, pp. 329-332, 2005.
[21] A. Sorrentino, G. Ferrara, A. Gifuni and M. Migliaccio, "Antenna pattern in a multipath environment emulated in a reverberating chamber," *7th European Conference on Antennas and Propagation (EuCAP)*, Gothenburg, Sweden, 2013, pp. 3561-3565.
[22] V. M. Primiani, "On the robustness of cable shielding effectiveness measurements in reverberation chamber," *IEEE Instrumentation and Measurement Technology Conference Proceedings*, Ottawa, Canada, 2005, pp. 441-444.
[23] C. L. Holloway, D. A. Hill, M. Sandroni, J. M. Ladbury, J. Coder, G. Koepke, A. C. Marvin and Y. He, "Use of reverberation chambers to determine the shielding effectiveness of physically small, electrically large enclosures and cavities," *IEEE Transactions on Electromagnetic Compatibility*, vol. 50, no. 4, pp. 770-782, Nov. 2008.
[24] C. L. Holloway, D. A. Hill, J. Ladbury, G. Koepke and R. Garzia, "Shielding effectiveness measurements of materials using nested reverberation chambers," *IEEE Transactions on Electromagnetic Compatibility*, vol. 45, no. 2, pp. 350-356, May 2003.
[25] I. D. Flintoft, S. J. Bale, S. L. Parker, A. C. Marvin, J. F. Dawson and M. P. Robinson, "On the measurable range of absorption cross section in a reverberation chamber," *IEEE Transactions on Electromagnetic Compatibility*, vol. 58, no. 1, pp. 22-29, Feb. 2016.
[26] D. Senic, A. Šarolić, Z. M. Jóskiewicz and C. L. Holloway, "Absorption cross-section measurements of a human model in a reverberation chamber," *IEEE Transactions on Electromagnetic Compatibility*, vol. 58, no. 3, pp. 721-728, Jun. 2016.
[27] Z. Tian, Y. Huang, Y. Shen and Q. Xu, "Efficient and accurate measurement of absorption cross section of a lossy object in reverberation chamber using two one-antenna methods," *IEEE Transactions on Electromagnetic Compatibility*, vol. 58, no. 3, pp. 686-693, Jun. 2016.
[28] G. Lerosey and J. de Rosny, "Scattering cross section measurement in reverberation chamber," *IEEE Transactions on Electromagnetic Compatibility*, vol. 49, no. 2, pp. 280-284, May 2007.
[29] S. Lalléchère, I. El Baba, P. Bonnet and F. Paladian, "Total scattering cross section improvements from electromagnetic reverberation chambers modeling and stochastic formalism," *Proceedings of the 5th European Conference on Antennas and Propagation (EUCAP)*, Rome, 2011, pp. 81-85.
[30] I. E. Baba, S. Lalléchère, P. Bonnet, J. Benoit and F. Paladian, "Computing total scattering cross section from 3-D reverberation chambers time modeling," *Asia-Pacific Symposium on Electromagnetic Compatibility*, Singapore, 2012, pp. 585-588.
[31] H. G. Krauthauser, "On the measurement of total radiated power in uncalibrated reverberation chambers," *IEEE Transactions on Electromagnetic Compatibility*, vol. 49, no. 2, pp. 270-279, May 2007.
[32] C. Orlenius, P. Lioliou, M. Franzen and P. Kildal, "Measurements of total radiated power of UMTS phones in reverberation chamber," *The Second European Conference on Antennas and Propagation (EuCAP)*, Edinburgh, 2007, pp. 1-6.
[33] K. A. Remley, J. Dortmans, C. Weldon, R. D. Horansky, T. B. Meurs, C. –M. Wang, D. F. Williams, C. L. Holloway and P. F. Wilson, "Configuring and verifying reverberation chambers for testing cellular wireless devices," *IEEE Transactions on Electromagnetic Compatibility*, vol. 58, no. 3, pp. 661-672, Jun. 2016.
[34] C. Orlenius, P. -. Kildal and G. Poilasne, "Measurements of total isotropic sensitivity and average fading sensitivity of CDMA phones in reverberation chamber," *IEEE Antennas and Propagation Society International Symposium*, Washington, DC, 2005, pp. 409-412, vol. 1A.
[35] M. Andersson, C. Orlenius and P. Kildal, "Three fast ways of measuring receiver sensitivity in a reverberation chamber," *International Workshop on Antenna Technology: Small Antennas and Novel Metamaterials*, Chiba, 2008, pp. 51-54.
[36] R. J. Pirkl, K. A. Remley and C. S. L. Patane, "Reverberation chamber measurement correlation," *IEEE Transactions on Electromagnetic Compatibility*, vol. 54, no. 3, pp. 533-545, Jun. 2012.